

## Doping-driven magnetic instabilities and quantum criticality of NbFe<sub>2</sub>

D. A. Tompsett,<sup>\*</sup> R. J. Needs, F. M. Grosche, and G. G. Lonzarich*Cavendish Laboratory, University of Cambridge, JJ Thomson Avenue, Cambridge CB3 0HE, United Kingdom*

(Received 21 June 2010; revised manuscript received 5 October 2010; published 25 October 2010)

Using density-functional theory we investigate the evolution of the magnetic ground state of NbFe<sub>2</sub> due to doping by Nb-excess and Fe-excess. We find that nonrigid-band effects due to the contribution of Fe *d* states to the density of states at the Fermi level are crucial to the evolution of the magnetic phase diagram. Furthermore, the influence of disorder is important to the development of ferromagnetism upon Nb doping. These findings give a framework in which to understand the evolution of the magnetic ground state in the temperature-doping phase diagram. We investigate the magnetic instabilities in NbFe<sub>2</sub>. We find that explicit calculation of the Lindhard function,  $\chi_0(\mathbf{q})$ , indicates that the primary instability is to finite  $\mathbf{q}$  antiferromagnetism driven by Fermi-surface nesting. Total-energy calculations indicate that  $\mathbf{q}=0$  antiferromagnetism is the ground state. We discuss the influence of competing  $\mathbf{q}=0$  and finite  $\mathbf{q}$  instabilities on the presence of the non-Fermi-liquid behavior in this material.

DOI: [10.1103/PhysRevB.82.155137](https://doi.org/10.1103/PhysRevB.82.155137)

PACS number(s): 71.20.Be, 75.10.Lp

### I. INTRODUCTION

Materials that exhibit magnetic phase transitions that may be tuned to zero temperature are strong candidates for the formation of novel ordered states around the quantum-critical point. These novel states rely upon the breakdown of assumptions that underpin the Fermi-liquid (FL) theory of metals when the magnetic interactions become extended in space and time. Such a situation is possible at a magnetic quantum critical point (QCP) and may lead to the formation of new phases of matter that are potentially technologically valuable. The formation of superconductivity in cuprates and iron-pnictides near magnetic phase transitions are among the phenomena that motivate us to understand materials where magnetic interactions are potentially of crucial importance.

The metallic compound NbFe<sub>2</sub> has been of interest to researchers for decades due to its rich magnetic-phase diagram. Initially, stoichiometric NbFe<sub>2</sub> was thought to be either paramagnetic or ferromagnetic (FM).<sup>1,2</sup> However, subsequent NMR (Ref. 3) and magnetization measurements<sup>4</sup> have been interpreted as showing spin-density-wave (SDW) order with a Néel temperature  $T_N \approx 10$  K.

Studies of the doping evolution of the phase diagram have shown that this spin-density-wave state is very sensitive to changes in stoichiometry. Studies of doping in Nb<sub>1-y</sub>Fe<sub>2+y</sub> with either Nb-excess ( $y < 0$ ) or Fe-excess ( $y > 0$ ) have shown that stoichiometric NbFe<sub>2</sub> becomes ferromagnetic upon either electron or hole doping.<sup>5</sup> Because of the close proximity of the reported SDW and ferromagnetism, NbFe<sub>2</sub> has long been considered a candidate material for the coexistence of SDW and ferromagnetic fluctuations.<sup>5,6</sup>

Recent experimental work has further probed the behavior of the temperature-doping phase diagram of high-purity NbFe<sub>2</sub> via measurements of the temperature dependence of resistivity, specific heat, and magnetic susceptibility.<sup>7,8</sup> The resulting phase diagram is shown in Fig. 1. Importantly, these refined measurements indicate the presence of a quantum-critical point as the reported SDW collapses when NbFe<sub>2</sub> is tuned away from stoichiometry by Nb-excess. At this critical point, intriguing non-Fermi-liquid behavior in

the material has been demonstrated. Wada *et al.*<sup>9</sup> had previously reported an enhanced electronic specific heat in the late 1980s. This behavior has been confirmed by recent measurements<sup>8,10,11</sup> that describe the non-Fermi-liquid behavior in more detail. They show at low temperatures near the quantum-critical point the presence of a logarithmic divergence of the specific heat and a  $\rho \propto T^{3/2}$  dependence in the resistivity.

Further NMR and magnetization studies have confirmed the presence of antiferromagnetism (AFM) at stoichiometry<sup>5,12,13</sup> but neutron-diffraction<sup>7,11</sup> studies have been unable to determine the magnetic order. Therefore, studying the electronic and magnetic properties of this material with electronic-structure calculations may aid our understanding and has been addressed previously.<sup>14–16</sup> Total-energy calculations with the frozen-core approximation<sup>15</sup> suggested a paramagnetic ground state while work with the linear muffin-tin-orbital method with shape approximations<sup>16</sup>

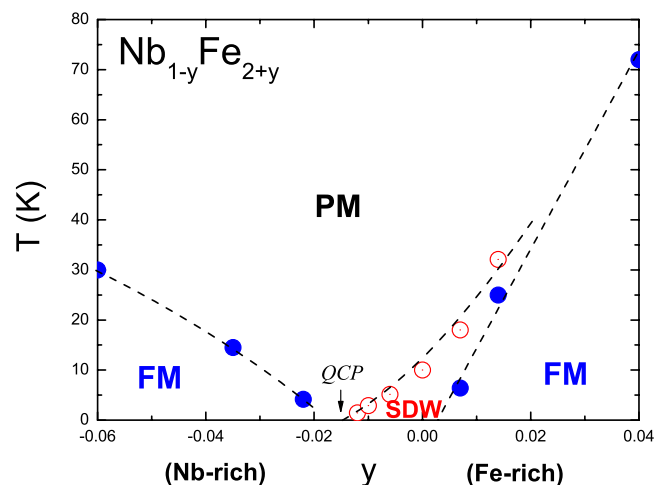


FIG. 1. (Color online) Phase diagram for Nb<sub>1-y</sub>Fe<sub>2+y</sub> (Ref. 7). By adjusting the precise composition within a narrow range, NbFe<sub>2</sub> can be tuned from FM ( $y > 0.01$ ) via an intermediate SDW modulated state to a QCP ( $y \approx -0.015$ ).

suggested an antiferromagnetic ground state nearly degenerate with a paramagnetic state.

Recent work by Subedi and Singh<sup>17</sup> has discussed in detail the magnetic interactions of local-moment configurations within the unit cell of stoichiometric NbFe<sub>2</sub>. NbFe<sub>2</sub> exhibits significant exchange splitting of the 3*s* core levels.<sup>18</sup> This indicates the presence of local-moment fluctuations as is also found in the Fe-based superconductors.<sup>19</sup> Subedi *et al.* found that the magnetism has itinerant character due to the dependence of the size of the moments on the magnetic configuration. Also, a ferrimagnetic ground state was found to be most favorable. Furthermore large moments  $\sim 1 \mu_B$  were obtained, which far exceed the  $\sim 0.02 \mu_B$  inferred from experiment. In this study we further address the magnetic ground state of this material using the full-potential methods in WIEN2K.<sup>20</sup> We consider the doping dependence of the ground state and discuss the magnetic interactions that may be key to the critical behavior in this material. Our findings for the ground state are used to discuss the driving forces behind the rich magnetic-phase diagram and the role of magnetism in the intriguing non-Fermi-liquid behavior of this material.

We begin our analysis by considering the electronic structure of stoichiometric NbFe<sub>2</sub>. All calculations are performed using the generalized-gradient approximation- (GGA-) Perdew-Burke-Ernzerhof (PBE) (Ref. 21) correlation functional. We have used the experimental lattice parameters.<sup>7</sup> For stoichiometric NbFe<sub>2</sub>  $a=4.8401(2) \text{ \AA}$  and  $c=1.8963(6) \text{ \AA}$ . All results presented were obtained using  $RK_{\text{max}}=8$ ,  $G_{\text{max}}=16$ , and Indices of the Fast Fourier Transform grid (IFFT) factor=4.0. Here,  $RK_{\text{max}}$  determines the matrix size ( $K_{\text{max}}$  is the plane wave cutoff and  $R$  is the smallest of the atomic sphere radii),  $G_{\text{max}}$  is the maximum wave vector in the charge-density Fourier expansion, and IFFT determines the size of the mesh for the calculation of the exchange-correlation potential in the interstitial region. The Fermi surface and charge densities were calculated from a  $43 \times 43 \times 23$  grid of  $k$  points. The radii of the muffin tins were  $2.12a_0$  for Fe and  $2.15a_0$  for Nb.

## II. CRYSTAL AND BONDING STRUCTURE

NbFe<sub>2</sub> crystallizes in the C14 Laves phase which has the MgZn<sub>2</sub> hexagonal structure. The crystal structure is shown in Fig. 2. The Fe atoms form a layered structure of a kagome lattice (6*h* sites) separated by Fe (2*a* sites) atoms centered on the line between alternate kagome triangles. The Nb atoms occupy the interstices in this Fe structure and lie slightly out of plane with respect to the Fe(2*a*) sites. The site symmetries have internal degrees of freedom: Nb at  $4f(1/3, 2/3, x)$  and Fe at  $2a(0,0,0)$  and  $6h(y,2y,3/4)$ . In our calculation of stoichiometric NbFe<sub>2</sub> we have relaxed these internal parameters resulting in  $x=0.0657$  and  $y=0.1705$ .

It is worth considering this crystal structure in further detail since its properties affect the bonding, doping impurity location, and the magnetic coupling. In Fig. 3(a) we show an extended view of the crystal structure along the *c* axis. We can see that the blue Fe(2*a*) atoms only coordinate every second triangle of the kagome structure formed by the

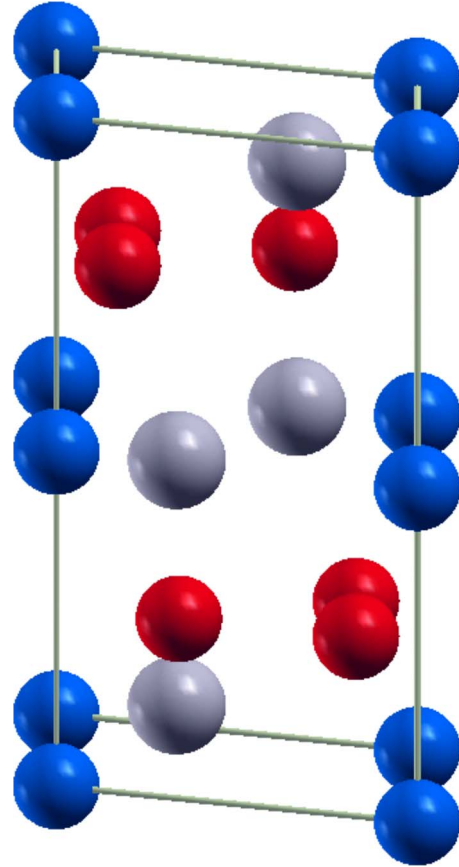


FIG. 2. (Color online) Crystal structure of NbFe<sub>2</sub>. Fe(6*h*) red, Fe(2*a*) blue, and Nb gray.

Fe(6*h*) sites. To emphasize this we have separated the colors of the upper and lower kagome layers into red and green. The presence of the Fe(2*a*) atoms coordinating every second kagome triangle means that the bonding between the pairs of Fe(6*h*) atoms in the kagome layers will not be the same. In Fig. 3(b) we show charge-density contours within the kagome layer. As we can see the bonding between Fe(6*h*) sites varies significantly. Effectively the presence of the Fe(2*a*) sites draws away charge density into the out of plane

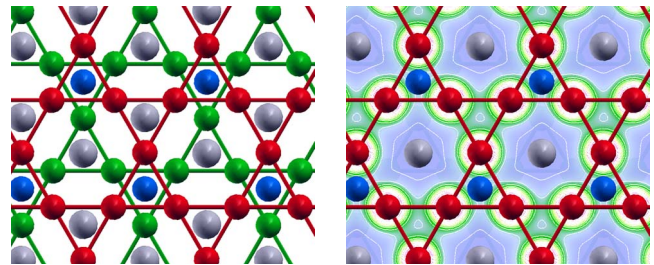


FIG. 3. (Color online) Crystal Structure of NbFe<sub>2</sub> at left. View shown along the *c* axis. The upper and lower kagome layers formed by the Fe(6*h*) sites have been separated into red and green, respectively. Fe(6*h*) red (upper kagome), Fe(6*h*) green (lower kagome), Fe(2*a*) blue, and Nb gray. In the right figure we show charge-density contours in the upper kagome plane. The charge density for kagome triangles coordinated with Fe(2*a*) sites is inequivalent to those with no coordination.

TABLE I. Interatomic bond distances for stoichiometric NbFe<sub>2</sub>. In each case we show the shortest distance between the two given sites.

Sites	Distance (Å)
Fe(2a)-Fe(6h)	2.42
Fe(6h)-Fe(6h)	2.37
Fe(2a)-Fe(2a)	3.95
Nb-Fe(2a)	2.84
Nb-Fe(6h)	2.81
Nb-Nb	2.89

Fe(2a)-Fe(6h) bonds and starves the bonds in the kagome triangles that are coordinated with an Fe(2a) site.

In Table I we show the interatomic bond distances. Significantly, among the Fe sites, the nearest-neighbor distances from Fe(2a) and Fe(6h) sites are similar. Therefore upon Nb doping, the preferred dopant site is likely to be determined by the bonding network of the Fe cage rather than the volume available at the site. We investigate this via total-energy calculations in the following section.

The density of states for nonmagnetic NbFe<sub>2</sub> is shown in Fig. 4 and agrees with the results of previous studies.<sup>14,17</sup> We also show the partial density of states by atomic site. The partial density of states for Fe(2a) *d* and Fe(6h) *d* sites possess similar structure, which is consistent with their strong bonding exhibited in the charge density. The Fe *d* states dominate the structure at the Fermi level. In contrast the Nb *d* character contributes far less structure to the overall density of states. This reflects the role of Nb as an electron donor in the system.

Clearly the Fermi level lies near a depression in the density of states which has been cited as important to the formation of a SDW at stoichiometry.<sup>17</sup> The density of states at  $E_F$  is 3.6 eV<sup>-1</sup> FU<sup>-1</sup>. In a rigid-band approximation the impact of doping a small amount of holes (e.g., Nb doping) will raise the total density of states and promote the development of ferromagnetism as is seen in its doping-phase diagram experimentally.<sup>8</sup> However, if we take the same rigid-band approach to electron doping, such as in the Fe-doped system,

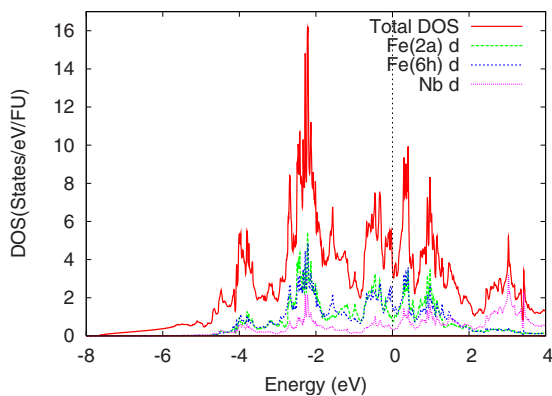


FIG. 4. (Color online) Nonmagnetic calculated DOS for NbFe<sub>2</sub>. The Fermi level is set to 0 eV.

then the density of states is expected to fall. This is in conflict with the experimental phase diagram (see Fig. 1), which shows the formation of ferromagnetism with small amounts of Fe doping. Therefore, effects beyond rigid-band shifts of  $E_F$  may be in operation and we attempt to explore these in the following section.

### III. DOPING DEPENDENCE OF THE FERROMAGNETIC INSTABILITY

We may evaluate the proximity of the system to ferromagnetism within Stoner theory,<sup>22</sup> where if  $N(E_F)I > 1$  then a material is unstable to ferromagnetism. It has been shown<sup>17</sup> that if we assume a typical interaction<sup>23,24</sup>  $I \sim 0.7-0.9$  eV then we obtain a Stoner enhancement of  $[1 - N(E_F)I]^{-1} \sim 3$  for stoichiometric NbFe<sub>2</sub>. Experimentally,<sup>8,11</sup> however, comparing the measured susceptibility with the band-structure value of  $N(E_F)$  indicates a Stoner enhancement  $[1 - N(E_F)I]^{-1} > 100$ . This suggests first, that the interaction scale may be unusually large in NbFe<sub>2</sub>,  $I > 1$  eV. Second, very slight increases in the value of  $N(E_F)$  of order a few percent should drive NbFe<sub>2</sub> to a ferromagnetic instability. In this section we utilize doped supercell calculations to investigate the evolution of  $N(E_F)$  with both hole (Nb) and electron (Fe) doping. We note that doped NbFe<sub>2</sub> samples are disordered as is evidenced by the significant increases in the low-temperature resistivities that occur upon doping.<sup>7</sup> For these calculations we have employed the lattice parameters derived from experiment<sup>7</sup> and relaxed all internal coordinates. We consider the nonmagnetic density of states in order to apply the Stoner framework.

First, we consider hole doping on the Nb-rich side of the phase diagram of Nb<sub>1-y</sub>Fe<sub>2+y</sub>. We consider doping corresponding to  $y = -0.065$  Nb rich Nb<sub>1.065</sub>Fe<sub>1.935</sub>. This state is formed by substituting one Nb atom for an Fe atom in a 2 × 2 supercell and lies beyond the formation of ferromagnetism in the experimental phase diagram. If we were to apply the rigid-band approximation to the density of states shown in Fig. 4, then we expect that for Nb<sub>1.065</sub>Fe<sub>1.935</sub> the density of states at the Fermi level,  $N(E_F)$ , will rise to 5.4 eV<sup>-1</sup> FU<sup>-1</sup>. Therefore the system would satisfy the Stoner criterion,  $N(E_F)I > 1$ , for ferromagnetism. Clearly, since there are the two inequivalent Fe(2a) and Fe(6h) sites, then the Nb might be doped at either one. We have performed supercell calculations with the Nb atom substituted at both sites. Nonmagnetic total-energy calculation for the 2 × 2 supercell indicated that for substitution at the Fe(6h) site the total energy is  $\sim 6.8$  eV/FU lower than that when we substitute at the Fe(2a) site. Therefore, the total energy strongly favors substitution at the Fe(6h) site.

In Fig. 5(a) we show the calculated density of states for Nb-rich Nb<sub>1.065</sub>Fe<sub>1.935</sub> with the Nb substituted on the Fe(6h) site. Here we find that  $N(E_F) = 3.8$  eV<sup>-1</sup> FU<sup>-1</sup>. This is a smaller rise than that predicted by the rigid-band approximation but probably still large enough to satisfy the criterion for the formation of ferromagnetism under Stoner theory. If we inspect the projected density of states for the Nb impurity and an Fe(6h) site shown in the same figure, then we can see a mechanism for this result. The Fe(6h) site contributes sig-



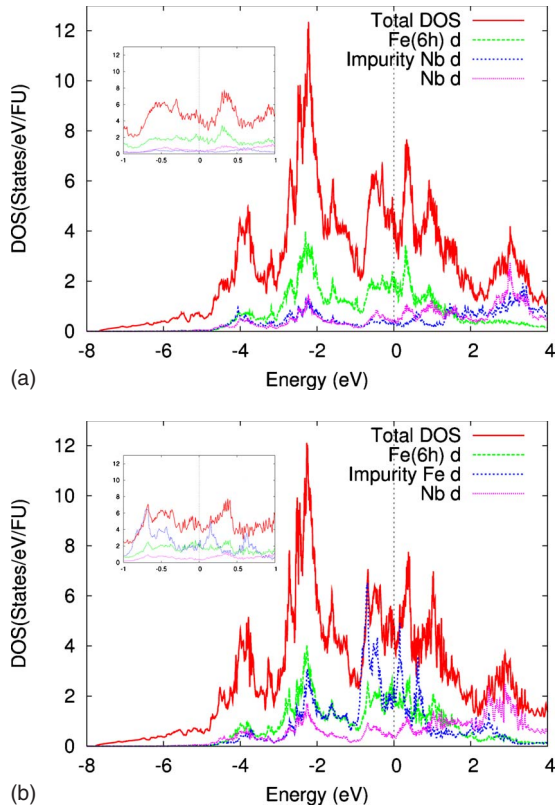


FIG. 5. (Color online) Nonmagnetic calculated DOS for (a) Nb-rich  $\text{Nb}_{1.065}\text{Fe}_{1.935}$  and for (b) Fe-rich  $\text{Nb}_{0.935}\text{Fe}_{2.065}$ . The insets show the same data on an expanded scale around the Fermi level. The Fermi level is set to 0 eV.

nificant structure to the density of states near the Fermi level. As a result when we dope a Nb onto a Fe(6h) site, not only are we removing valence electrons from the system but we are also decreasing the contribution from Fe(6h) sites to the density of states at the Fermi level. The importance of the structure of Fe  $d$  states has been noted by Inoue *et al.*<sup>25</sup> in tight-binding calculations incorporating impurity atoms. Consequently, the density of states at the Fermi level from our doped supercell calculation is lower than that expected in the rigid-band approximation.

Next we consider electron doping on the Fe-rich side of the phase diagram of  $\text{Nb}_{1-y}\text{Fe}_{2+y}$ . We consider doping corresponding to  $y=0.065$  Fe-rich  $\text{Nb}_{0.935}\text{Fe}_{2.065}$ . This state is formed by substituting one Fe atom for a Nb atom in a  $2 \times 2$  supercell and is well within the ferromagnetic region of the experimental phase diagram. However, according to the rigid-band approximation, this doping would actually produce a small fall in the density of states at the Fermi level to  $N(E_F)=3.5 \text{ eV}^{-1} \text{FU}^{-1}$ . This is due to the fact that the Fermi level effectively moves higher in energy in Fig. 4 and as a result the density of states falls deeper into the trough near the Fermi level. Therefore, in the rigid-band approximation the Stoner criterion would not be satisfied and ferromagnetism would not result. In Fig. 5(b) we show the density of states from our supercell calculation of  $\text{Nb}_{0.935}\text{Fe}_{2.065}$ . Critically, the density of states at the Fermi level actually rises to  $N(E_F)=4.5 \text{ eV}^{-1} \text{FU}^{-1}$ . This is due to the fact, that despite the addition of valence electrons, the Fe dopant contributes

increased structure to the density of states at  $E_F$ . To illustrate this we show in Fig. 5(b) the projected density of states for the Fe dopant at the Nb site. We see that, unlike Nb, this Fe dopant contributes a form to the density of states that is very similar to that of an Fe(6h) site.

Also, we have made a simple approximation to the disorder by applying a Gaussian broadening of width 41 meV to our density of states to reflect the decreased lifetime of electrons in the states near the Fermi level due to disorder. This is calculated from the measured low-temperature resistivity in a Drude approximation.<sup>7,26,27</sup> In Nb-rich  $\text{Nb}_{1.065}\text{Fe}_{1.935}$  we find that  $N(E_F)=4.6 \text{ eV}^{-1} \text{FU}^{-1}$ . The reason for the large increase compared to  $N(E_F)=3.8 \text{ eV}^{-1} \text{FU}^{-1}$  found without this broadening may be ascertained from the inset to Fig. 5(a). The Fermi level lies in a sharp dip in the density of states and therefore disorder-induced broadening is likely to smear out this structure and increase  $N(E_F)$ . This suggests that disorder may be important to the development of ferromagnetism upon Nb doping. In contrast  $N(E_F)$  is found to be insensitive to the broadening for Fe-rich  $\text{Nb}_{0.935}\text{Fe}_{2.065}$ . The influence of disorder may also explain discrepancies between experimentally determined phase diagrams where some work<sup>5</sup> shows the development of ferromagnetism for lower Nb dopings than in more recent studies.<sup>7,8</sup> This indicative result invites further work on the description of disorder with approaches such as the coherent-potential approximation.<sup>28–31</sup> A further consideration in such work may be how the interaction,  $I$ , changes with disorder.

These findings illustrate several important points about the evolution of the temperature-doping phase diagram. (1) A rigid-band approximation is not sufficient to understand the evolution to ferromagnetism, particularly for electron doping. (2) The type of dopant will be critical to the character of this phase diagram. This is essentially because the fine structure of this phase diagram is strongly affected by the contributions to the density of states at the Fermi level from Fe  $d$  states. (3) The presence of disorder may be important to the development of ferromagnetism upon Nb doping.

We have also undertaken calculations for dopings of  $y = \pm 0.0325$  using  $2 \times 2 \times 2$  supercells. These calculations deliver results with the same qualitative conclusions. For example we considered doping corresponding to  $y=0.0325$  Fe-rich  $\text{Nb}_{0.9675}\text{Fe}_{2.0325}$ . This state is formed by substituting one Fe atom for a Nb atom in a  $2 \times 2 \times 2$  supercell. Applying the rigid-band approximation would result in a fall from  $N(E_F)=3.6 \text{ eV}^{-1} \text{FU}^{-1}$  in stoichiometric  $\text{NbFe}_2$  to  $N(E_F)=3.0 \text{ eV}^{-1} \text{FU}^{-1}$ . Our supercell calculation for Fe-rich  $\text{Nb}_{0.9675}\text{Fe}_{2.0325}$  indicates  $N(E_F)=4.1 \text{ eV}^{-1} \text{FU}^{-1}$  and supports the formation of ferromagnetism as shown in the experimental phase diagram of Fig. 1.

#### IV. FERMI SURFACE AND MAGNETIC INSTABILITIES

To further our understanding of the complex evolution of the magnetic phase diagram with doping we here consider the magnetic interactions active in stoichiometric  $\text{NbFe}_2$ , which has experimentally been interpreted as having SDW character. The previous work of Subedi and Singh<sup>17</sup> has considered the interaction of different magnetic orders within the

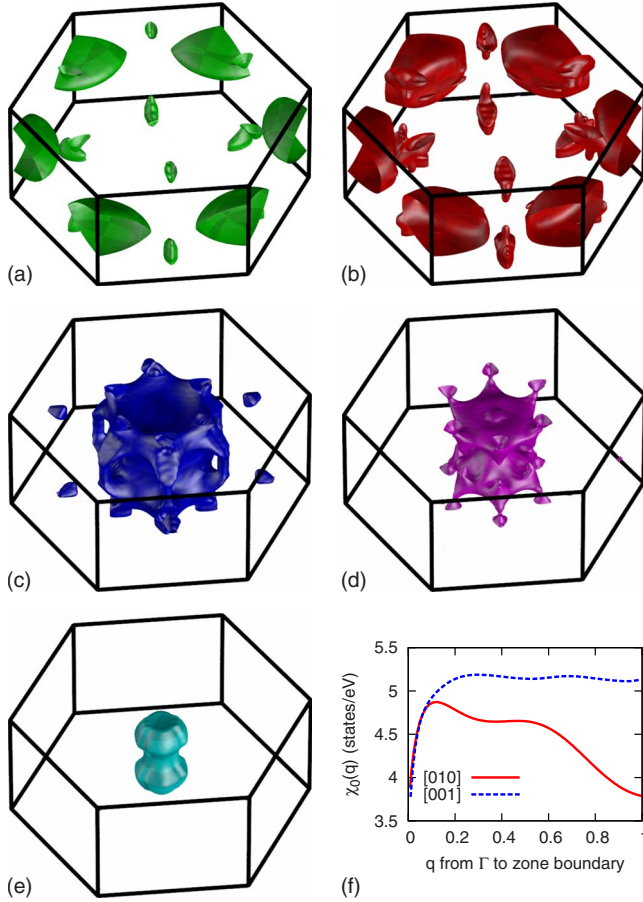


FIG. 6. (Color online) In (a)–(e) we show the nonmagnetic Fermi surface of NbFe<sub>2</sub>. The flat sections of Fermi surface in bands 81 and 82 show potential for nesting. In (f) we show the noninteracting susceptibility,  $\chi_0(\mathbf{q})$ , for NbFe<sub>2</sub> along both the [010] and [001] directions. The large flat enhancement in  $\chi_0(\mathbf{q})$  along the [001] direction indicates the potential importance of large  $\mathbf{q}$  magnetic instabilities. The flat sections of the Fermi surface of the bands 82 and 83 are the dominant contribution to the susceptibility at large  $\mathbf{q}$ . A similar phenomenon is observed due to the cubic shaped Fermi surface in TiBe<sub>2</sub> (Ref. 32).

unit cell under the local spin-density approximation (LSDA).

The Fermi surface of metallic materials is crucial in the understanding of their properties. In Fig. 6 we show the calculated nonmagnetic Fermi surface for stoichiometric NbFe<sub>2</sub> which agrees well with previous work.<sup>17</sup> We reproduce this Fermi surface to emphasize the importance of features that may be important to the magnetic instabilities of the system. Five sheets make up this Fermi surface which is strongly three-dimensional (3D). We consider the nonmagnetic Fermi surface because we are interested in the magnetic instabilities as we approach the QCP, where the static moment and spin splitting of the Fermi surface approach zero.

We proceed by calculating  $\chi_0(\mathbf{q})$  using the technique of Romberg integration

$$\chi_0(\mathbf{q}) = \sum_{n,\mathbf{k}} M_{\mathbf{k},\mathbf{k}+\mathbf{q}}^2 \left[ \frac{f_{n,\mathbf{k}} - f_{n,\mathbf{k}+\mathbf{q}}}{\varepsilon_{n,\mathbf{k}+\mathbf{q}} - \varepsilon_{n,\mathbf{k}}} \right]. \quad (1)$$

Here, the sum is over all bands up to 1 eV above the Fermi level,  $n$ , and wave vectors  $\mathbf{k}$ .  $M$  are the matrix elements and

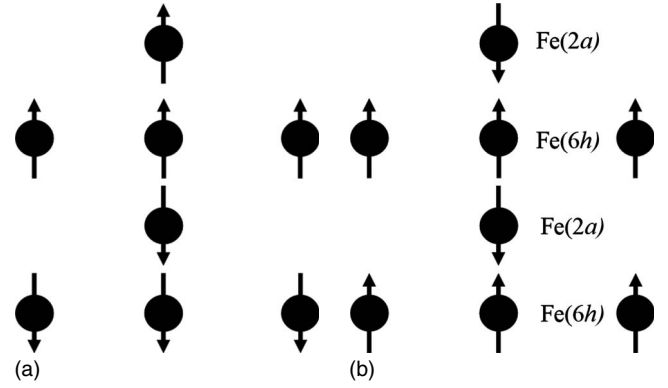


FIG. 7. Schematic diagram of the spin configuration for (a) AFM2  $\mathbf{q}=0$  antiferromagnetism and (b) AFM3 the lowest energy state found by Subedi and Singh (Ref. 17). Only Fe atoms are shown and the  $2a$  and  $6h$  rows are as indicated.

$f$  is the Fermi occupation function. No increased lifetime broadening was applied. In Fig. 6(f) we show the susceptibility for  $\mathbf{q}$  parallel to [010] and for  $\mathbf{q}$  parallel to [001]. We have included only *intra*band contributions for which we may to a good approximation set the matrix element  $M=1$ . Both susceptibilities rise steeply away from  $\mathbf{q}=0$ . Along [010], the susceptibility peaks at a small wave vector,  $\mathbf{q} \approx [00.0750]\pi/b$ , and then falls monotonically until the zone boundary is reached. Along [001] the susceptibility rises to a higher level than that in-plane  $\approx 40\%$  above that at  $\mathbf{q}=0$ . It then levels off to an essentially constant value until the zone boundary is reached. Enhancements at finite  $\mathbf{q}$  are consistent with previous work.<sup>17</sup> From these calculations it appears likely that finite  $\mathbf{q}$  instabilities, particularly along [001], may be important in this system.

We note also, that in the absence of spin-orbit effects the matrix element for *inter*band contributions is  $M=0$  at  $\mathbf{q}=0$  due to orthogonality, then the inclusion of interband contributions will enhance the finite  $\mathbf{q}$  instabilities shown in Fig. 6(f). Inspection of the contributions of each Fermi-surface sheet shows that the rising value of  $\chi_0(\mathbf{q})$  along [001] is due largely to bands 82 and 83. This results from the presence of the very flat sections of surface that they possess. These flat sections nest strongly as they are translated by the wave vector  $\mathbf{q}$ . This behavior is very similar to the large finite  $\mathbf{q}$  instability found due to the flat sides of the cubelike Fermi surfaces in metamagnetic TiBe<sub>2</sub>.<sup>32</sup>

We also compare competing magnetic ground states by performing total-energy calculations. Our total-energy calculations consider several magnetic states including (1) nonmagnetic, (2) ferromagnetic, (3) AFM1 which is commensurate along the  $c$  axis as suggested by the calculation of  $\chi_0(\mathbf{q})$ , (4) AFM2 which is  $\mathbf{q}=0$  antiferromagnetism of the type found in the C14 Laves material TiFe<sub>2</sub>, and (5) AFM3 which is the lowest energy state found by Subedi and Singh<sup>17</sup> We show the spin configurations associated with some of these orders in Fig. 7.

For the energy evaluation we have used 10,000  $k$  points in the Brillouin zone and the GGA-PBE exchange-correlation functional. As shown in Table II we find that the lowest energy state corresponds to  $\mathbf{q}=0$  antiferromagnetism of the

TABLE II. Comparative energetics of magnetic states. For the ferromagnetic state the total magnetic moment is  $2.34 \mu_B$  per formula unit. In the ferromagnetic state the Nb is found to also carry a small moment  $\approx 0.2 \mu_B$  which is antiferromagnetically coupled to the Fe moments.

	Energy (meV/FU)	Fe(2a) [ $\mu(\mu_B)$ ]	Fe(6h) [ $\mu(\mu_B)$ ]
NM	0	0	0
FM	-84	1.1	1.5
AFM1	-96	1.6	1.4
AFM2	-104	1.6	1.5
AFM3	-97	1.8	0.98

type found experimentally in the C14 Laves material  $\text{TiFe}_2$ .<sup>33</sup> However, our results indicate that the Fe(2a) possesses a moment while the experiments on  $\text{TiFe}_2$  indicate no ordered moment. In this calculation the second lowest energy state is then the ferrimagnetic state found to have the lowest energy by Subedi and Singh<sup>17</sup> The use of the LSDA correlation functional in that study results in a different configuration of spins for the lowest energy state.

For the SDW order AFM1 corresponding to the peak in  $\chi_0(\mathbf{q})$  along the  $c$  axis we find a lower energy than that obtained for ferromagnetism but not lower than the configurations within the unit cell. The ground-state calculation for these SDW configurations also produces large moments and suggests that the energy gain is again dominated not by the Fermi-surface nesting but by the Hund's coupling.

Importantly, the ordered moment below the SDW transition ( $< 0.02 \mu_B$ ) represents only a small fraction of the fluctuating moment.<sup>8</sup> Magnetic order is then expected to have a minor effect on the magnetic fluctuation spectrum and hence on the low-temperature properties, in particular, the non-Fermi-liquid low-temperature exponents. This is evidenced by the small size of the heat-capacity anomaly at  $T_N \approx 10$  K even in stoichiometric  $\text{NbFe}_2$ . Therefore, the presence of finite  $\mathbf{q}$  magnetic fluctuations may have an important role in producing the non-Fermi-liquid properties.

From spin-fluctuation theory, it is known that at an antiferromagnetic ( $\mathbf{q} \neq 0$ ) quantum-critical point the expected temperature dependence of the resistivity is  $\rho \propto T^{3/2}$  in the presence of sufficiently strong quenched disorder<sup>34</sup> while the leading-order term in the specific heat is linear in  $T$ . In contrast at a ferromagnetic critical point ( $\mathbf{q}=0$ ),  $\rho \propto T^{5/3}$  and the specific-heat diverges logarithmically. As shown in Table III, experiments on  $\text{NbFe}_2$  at its quantum critical point might suggest the presence of both ferromagnetic and antiferromagnetic spin fluctuations if we were able to treat these modes separately. Alternatively,  $\text{NbFe}_2$  may be entering into a new regime such as that found in the high-pressure region of the helimagnet  $\text{MnSi}$ .<sup>36</sup> It is possible that the presence of  $\mathbf{q}=0$  and finite  $\mathbf{q}$  instabilities in this material may combine to produce the unusual non-Fermi-liquid behavior. The prominence of such instabilities in  $\text{NbFe}_2$  is confirmed by both our calculation of the susceptibility in Fig. 6(f) and the total-energy calculations in Table II.

TABLE III. Results from spin-fluctuation theory (Ref. 35) in 3D shown alongside the experimental results for  $\text{NbFe}_2$  at its quantum critical point (Ref. 8). Results are shown for the standard FL, a system near a finite  $\mathbf{q}$  AFM instability and a system near an FM instability.

Property	FL	AFM	FM	$\text{NbFe}_2$
Specific heat (C)	$T$	$T$	$T \ln(T^*/T)$	$T \ln(T^*/T)$
Resistivity ( $\rho$ )	$T^2$	$T^{3/2}$	$T^{5/3}$	$T^{3/2}$

The interplay of Fermi-surface nesting along with other magnetic couplings in this system is shared with the Fe-based superconductors, where nesting is important along with other band-structure effects. The competition of these effects has been shown by Yildirim<sup>37</sup> to produce the structural phase transition in the Fe-based superconductors. In the  $\text{NbFe}_2$  system they may produce intriguing non-Fermi-liquid properties.

## V. SUMMARY AND DISCUSSION

The bonding structure of the Fe cages in  $\text{NbFe}_2$  is likely to be instrumental in producing the magnetic interactions that dominate the formation of its magnetic ground state. This bonding produces inequivalent character in the kagome triangles in the Fe(6h) layers.

We demonstrate that nonrigid-band effects must be considered in order to understand the evolution of the ground state as a function of doping. The contribution of Fe  $d$  states to the density of states at the Fermi level is shown to be critical to the production of a Stoner instability upon electron doping with Fe impurities. Therefore, it is expected that the nature of the electron dopant will be crucial to the evolution of the phase diagram. Also, the presence of disorder is likely to be important to the formation of ferromagnetism upon Nb doping.

We find that  $\text{NbFe}_2$  is close to both small and large  $\mathbf{q}$  magnetic instabilities. The noninteracting susceptibility indicates the potential importance of  $\mathbf{q} \neq 0$  instabilities. The electronic structure is highly three-dimensional but the possibilities for nesting of quasi-one-dimensional sections of the Fermi surface may provide crucial magnetic instabilities. Total-energy calculations indicate that spin configurations within the unit cell produce the lowest energy state.

The unusual non-Fermi-liquid critical exponents of  $\text{NbFe}_2$  may arise from the combination of  $\mathbf{q} \neq 0$  and  $\mathbf{q}=0$  instabilities. Further investigation as to how these instabilities may interplay will be necessary both theoretically and experimentally. Furthermore, the presence of such a large phase space for fluctuations is likely to complicate the formation of superconducting Cooper pairs in either the spin singlet or triplet channels.

## ACKNOWLEDGMENT

The authors would like to acknowledge useful discussions with J. B. Staunton.



\*dat36@cam.ac.uk

- <sup>1</sup>M. Nevitt, C. Kimball, and R. Preston, *Proceedings of the International Conference on Magnetism*, Nottingham, 1964 (The Institute of Physics and The Physical Society, London, 1964), Vol. 169, p. 137.
- <sup>2</sup>Y. Yamada, Y. Kitaoka, K. Asayama, and A. Sakata, *J. Phys. Soc. Jpn.* **53**, 3198 (1984).
- <sup>3</sup>Y. Yamada and A. Sakata, *J. Phys. Soc. Jpn.* **57**, 46 (1988).
- <sup>4</sup>Y. Yamada, R. Moru, K. Hirano, T. Hirotsuji, G. Obara, and T. Nakamura, *J. Magn. Magn. Mater.* **310**, 1812 (2007).
- <sup>5</sup>M. R. Crook and R. Cywinski, *J. Magn. Magn. Mater.* **140-144**, 71 (1995).
- <sup>6</sup>M. Shiga and Y. Nakamura, *J. Phys. Soc. Jpn.* **56**, 4040 (1987).
- <sup>7</sup>D. Moroni-Klementowicz, M. Brando, C. Albrecht, W. J. Duncan, F. M. Grosche, D. Grüner, and G. Kreiner, *Phys. Rev. B* **79**, 224410 (2009).
- <sup>8</sup>M. Brando, W. J. Duncan, D. Moroni-Klementowicz, C. Albrecht, D. Grüner, R. Ballou, and F. M. Grosche, *Phys. Rev. Lett.* **101**, 026401 (2008).
- <sup>9</sup>H. Wada, M. Hada, M. Shiga, and Y. Nakamura, *J. Phys. Soc. Jpn.* **59**, 701 (1990).
- <sup>10</sup>M. Brando, D. Moroni-Klementowicz, C. Albrecht, W. Duncan, D. Gruener, R. Ballou, B. Fak, and F. M. Grosche, Proceedings of 17th International Conference on Magnetism, Kyoto, Japan, 20–25 Aug., 2006; *J. Magn. Magn. Mater.* **310**, 852 (2007).
- <sup>11</sup>M. Brando, D. Moroni-Klementowicz, C. Albrecht, and F. Grosche, International Conference on Strongly Correlated Electron Systems, Vienna, Austria, 26–30 Jul., 2005; *Physica B* **378**, 111 (2006).
- <sup>12</sup>Y. Yamada, H. Nakamura, Y. Kitaoka, K. Asayama, K. Koga, A. Sakata, and T. Murakami, *J. Phys. Soc. Jpn.* **59**, 2976 (1990).
- <sup>13</sup>M. Kurisu, Y. Andoh, and Y. Yamada, Proceedings of the Yamada Conference XLV, the International Conference on the Physics of Transition Metals; *Physica B* **237-238**, 493 (1997).
- <sup>14</sup>S. Ishida, S. Asano, and J. Ishida, *J. Phys. Soc. Jpn.* **54**, 3925 (1985).
- <sup>15</sup>S. Asano and S. Ishida, *J. Phys. F: Met. Phys.* **18**, 501 (1988).
- <sup>16</sup>S. Asano and S. Ishida, *J. Phys.: Condens. Matter* **1**, 8501 (1989).
- <sup>17</sup>A. Subedi and D. J. Singh, *Phys. Rev. B* **81**, 024422 (2010).
- <sup>18</sup>J. F. van Acker, Z. M. Stadnik, J. C. Fuggle, H. J. W. M. Hoekstra, K. H. J. Buschow, and G. Stroink, *Phys. Rev. B* **37**, 6827 (1988).
- <sup>19</sup>F. Bondino, E. Magnano, M. Malvestuto, F. Parmigiani, M. A. McGuire, A. S. Sefat, B. C. Sales, R. Jin, D. Mandrus, E. W. Plummer, D. J. Singh, and N. Mannella, *Phys. Rev. Lett.* **101**, 267001 (2008).
- <sup>20</sup>K. Schwarz and P. Blaha, *Comput. Mater. Sci.* **28**, 259 (2003).
- <sup>21</sup>J. P. Perdew, K. Burke, and M. Ernzerhof, *Phys. Rev. Lett.* **77**, 3865 (1996).
- <sup>22</sup>E. Stoner, *Proc. R. Soc. London, Ser. A* **169**, 0339 (1939).
- <sup>23</sup>O. K. Andersen, J. Madsen, U. K. Poulsen, O. Jepsen, and J. Kollár, *Physica B & C* **86-88**, 249 (1977).
- <sup>24</sup>U. Poulsen, J. Kollar, and O. Andersen, *J. Phys. F: Met. Phys.* **6**, L241 (1976).
- <sup>25</sup>J. Inoue and M. Shimizu, *J. Magn. Magn. Mater.* **79**, 265 (1989).
- <sup>26</sup>C. M. Soukoulis and D. A. Papaconstantopoulos, *Phys. Rev. B* **26**, 3673 (1982).
- <sup>27</sup>L. R. Testardi and L. F. Mattheiss, *Phys. Rev. Lett.* **41**, 1612 (1978).
- <sup>28</sup>P. Soven, *Phys. Rev.* **156**, 809 (1967).
- <sup>29</sup>A. Gonis, *Green Functions for Ordered and Disordered Systems* (North-Holland, Amsterdam, 1992).
- <sup>30</sup>A. J. Pindor, W. M. Temmerman, and B. L. Gyorffy, *J. Phys. F: Met. Phys.* **13**, 1627 (1983).
- <sup>31</sup>I. Turek, V. Drchal, J. Kudrnovsky, M. Sob, and P. Weinberger, *Electronic Structure of Disordered Alloys, Surfaces and Interfaces* (Kluwer Academic, Boston, 1997).
- <sup>32</sup>T. Jeong, A. Kyker, and W. E. Pickett, *Phys. Rev. B* **73**, 115106 (2006).
- <sup>33</sup>P. J. Brown, J. Deportes, and B. Ouladdiaf, *J. Phys.: Condens. Matter* **4**, 10015 (1992).
- <sup>34</sup>R. Hlubina and T. M. Rice, *Phys. Rev. B* **51**, 9253 (1995).
- <sup>35</sup>T. Moriya, *Spin Fluctuations in Itinerant Electron Magnetism* (Springer-Verlag, Berlin, 1985).
- <sup>36</sup>C. Pfleiderer, D. Reznik, L. Pintschovius, H. von Lohneysen, M. Garst, and A. Rosch, *Nature* **427**, 227 (2004).
- <sup>37</sup>T. Yildirim, *Phys. Rev. Lett.* **101**, 057010 (2008).